


Structure–activity relationship studies of allosteric inhibitors of EYA2 tyrosine phosphatase

Jothi Anantharajan¹ | Nithya Baburajendran¹ | Grace Lin¹ | Yong Yao Loh¹ | Weijun Xu¹ | Nur Huda Binte Ahmad¹ | Shuang Liu^{1,2} | Anna E. Jansson¹ | John Wee Liang Kuan¹ | Elizabeth Yihui Ng¹ | Yee Khoon Yeo¹ | Alvin W. Hung¹ | Joma Joy¹ | Jeffrey Hill¹ | Heide L. Ford³ | Rui Zhao⁴ | Thomas H. Keller¹ | CongBao Kang¹ 

¹Experimental Drug Development Centre, Agency for Science, Technology and Research (A*STAR), Singapore

²Chemical Biology and Therapeutics Science, Broad Institute of MIT and Harvard, Cambridge, Massachusetts, USA

³Department of Obstetrics and Gynecology, University of Colorado Anschutz Medical Campus, Aurora, Colorado, USA

⁴Department of Biochemistry and Molecular Genetics, University of Colorado Anschutz Medical Campus, Aurora, Colorado, USA

Correspondence

Joma Joy, Thomas H. Keller, and CongBao Kang, Experimental Drug Development Centre, A*STAR, 10 Biopolis Road, #5-01, Singapore 138670.

Email: jjoy@eddc.a-star.edu.sg (J. J.), thkeller@eddc.a-star.edu.sg (T. H. K.), and cbkang@eddc.a-star.edu.sg (C. K.)

Funding information

This research was funded by Singapore Ministry of Health's National Medical Research Council under its open fund individual research grant (OFIRG17may050 and NMRC/OFIRG/0051/2017). Heide L. Ford is supported for inhibition of SIX1/EYA through National Institutes of Health grants NS108396 and CA224867.

Abstract

Human eyes absent (EYA) proteins possess Tyr phosphatase activity, which is critical for numerous cancer and metastasis promoting activities, making it an attractive target for cancer therapy. In this work, we demonstrate that the inhibitor-bound form of EYA2 does not favour binding to Mg²⁺, which is indispensable for the Tyr phosphatase activity. We further describe characterization and optimization of this class of allosteric inhibitors. A series of analogues were synthesized to improve potency of the inhibitors and to elucidate structure–activity relationships. Two co-crystal structures confirm the binding modes of this class of inhibitors. Our medicinal chemical, structural, biochemical, and biophysical studies provide insight into the molecular interactions of EYA2 with these allosteric inhibitors. The compounds derived from this study are useful for exploring the function of the Tyr phosphatase activity of EYA2 in normal and cancerous cells and serve as reference compounds for screening or developing allosteric phosphatase inhibitors. Finally, the co-crystal structures reported in this study will aid in structure-based drug discovery against EYA2.

KEYWORDS

allosteric inhibitor, EYA2, phosphatase inhibitor, protein binding, protein structure

Abbreviations: ED, EYA domain; EYA, eyes absent; HMB, helical bundle motif; IC₅₀, half-maximal inhibitory concentration; K_d, dissociation constant; PME, particle-mesh Ewald; SIX, sine oculis homeobox homolog.

1 | INTRODUCTION

Human sine oculis homeobox homolog (SIX) proteins are critical developmental transcription factors that bind DNA via nucleic acid recognition through a conserved homeodomain.¹ To mediate transcriptional activation, the SIX family of proteins interact with eyes absent (EYA) proteins to form bipartite transcriptional complexes. Most EYA proteins are critical for development and are downregulated in normal adult tissues.² Aberrant expression of EYA proteins is observed in numerous tumours, indicating that they may play a critical role in tumour progression.^{3–6} SIX/EYA complexes are known to activate critical pro-metastatic pathways; knockdown of EYA2 in SIX1-overexpressing breast cancer cells inhibits TGF- β signalling, epithelial-mesenchymal transition, and tumour initiating cell phenotypes.⁷ Disruption of interactions between SIX1 and EYA2 via introduction of a SIX1 point mutation at the binding interface of SIX1 and EYA2 inhibits metastasis in a xenograft model of breast cancer.⁸ A number of studies suggest that EYA2 might play important roles in lung cancer.^{9–12} The EYA2/SIX1 complex could be an important drug target, and disrupting EYA and SIX interactions is, therefore, of great interest in anticancer drug development.^{10,11,13,14} A crystal structure of SIX1/EYA2 complex was obtained, providing a structural basis to develop compounds that disrupt this protein–protein interaction.³ However, it has been noted that finding such inhibitors is a challenging task as the SIX1 binding pocket in EYA2 is shallow and hydrophilic.^{8,15}

The human EYA family of proteins consists of four members (EYAs 1–4) with high sequence homology and overlapping as well as differential expression across tissues.¹⁶ The N-terminal domain of the EYA proteins interacts with protein phosphatase 2A, which is required for the S/T/ phosphatase activity.³ The C-terminal domain contains a conserved EYA domain (ED), which is responsible for binding to SIX proteins and harbors an intrinsic Tyr phosphatase activity.^{16–18} Several groups have reported that the ED belongs to the phosphatase subgroup of the haloacid dehalogenase (HAD) superfamily, which are set apart from other phosphatases through their use of an aspartic acid as an active site residue, rather than a cysteine.¹⁹ Mg²⁺ is known to be critical for the Tyr phosphatase activity and folding of EYA proteins.¹⁹ We have shown that an allosteric inhibitor²⁰ is able to suppress the Tyr phosphatase activity of EYA2 by altering the conformation of the EYA2 ED. Inhibiting the Tyr phosphatase activity of EYA proteins could be a promising drug discovery strategy as this activity of EYA proteins has been shown to play a role in SIX1-mediated transcription,³ and is critical for transformation,

migration, invasion, and metastasis in breast cancer and lung cancer.^{20,21}

Tyrosine phosphatases are generally difficult drug targets, since their active site is flat and hydrophilic, and the transition state of the dephosphorylation step cannot be easily mimicked by organic compounds. An allosteric EYA2 inhibitor was identified through high throughput screening,²² and we confirmed its mechanism of action using X-ray crystallography.²⁰ This allosteric inhibitor has been utilized as a chemical probe to explore the function of EYA2 in cancer cell lines.²⁰ In this study, we report a detailed study of the molecular recognition of compounds in the allosteric pocket and the use of ¹⁹F-NMR spectroscopy to study the influence of Mg²⁺ on the conformational equilibrium. Our study demonstrates that it is feasible to develop EYA2 Tyr phosphatase inhibitors using the identified allosteric site.

2 | RESULTS

2.1 | Effect of Mg²⁺ on the inhibitor binding to EYA2 ED

The crystal structure of EYA2 ED-ETC-232 (named as 9987 in the previous publication²⁰) complex demonstrates that ETC-232 bound EYA2 ED does not bind to Mg²⁺, as inhibitor binding to the ED alters the conformation of residues critical for Mg²⁺ interactions.²⁰ Indeed, a previous study also showed that Mg²⁺ was able to reduce the binding affinity of ETC-232.²² We observed that the half-maximal inhibitory concentration (IC₅₀) of ETC-232 on the Tyr phosphatase activity of EYA2 ED was dependent on the concentration Mg²⁺. ETC-232 exhibited an IC₅₀ of 0.39 μ M when the concentration of Mg²⁺ was 5 μ M in the assay buffer while a higher IC₅₀ value was observed in our previous study²⁰ when 5 mM of Mg²⁺ was present (Figure 1a). The result is consistent with the notion that compound binding and Mg²⁺ binding compete with each other. To compare the IC₅₀ values of different compounds, the concentration of Mg²⁺ was set as 5 μ M in the assay buffer. We characterized the molecular interactions between EYA2 ED and ETC-232 in the absence and presence of Mg²⁺. The binding affinity of ETC-232 to EYA2 ED was shown to be 1.2 μ M as measured by ITC in the absence of Mg²⁺ (Figure 1b), consistent with the K_d observed for a similar compound with EYA2 ED.²² As ETC-232 contains a fluorine atom, we then used ligand-observed ¹⁹F-NMR to explore the effect of Mg²⁺ on its interaction with EYA2 ED. Free ETC-232 exhibited a single peak at approximately –112 ppm in the 1D ¹⁹F-NMR spectrum. The observed resonance with low intensity was due to its low solubility in solution. In the presence of

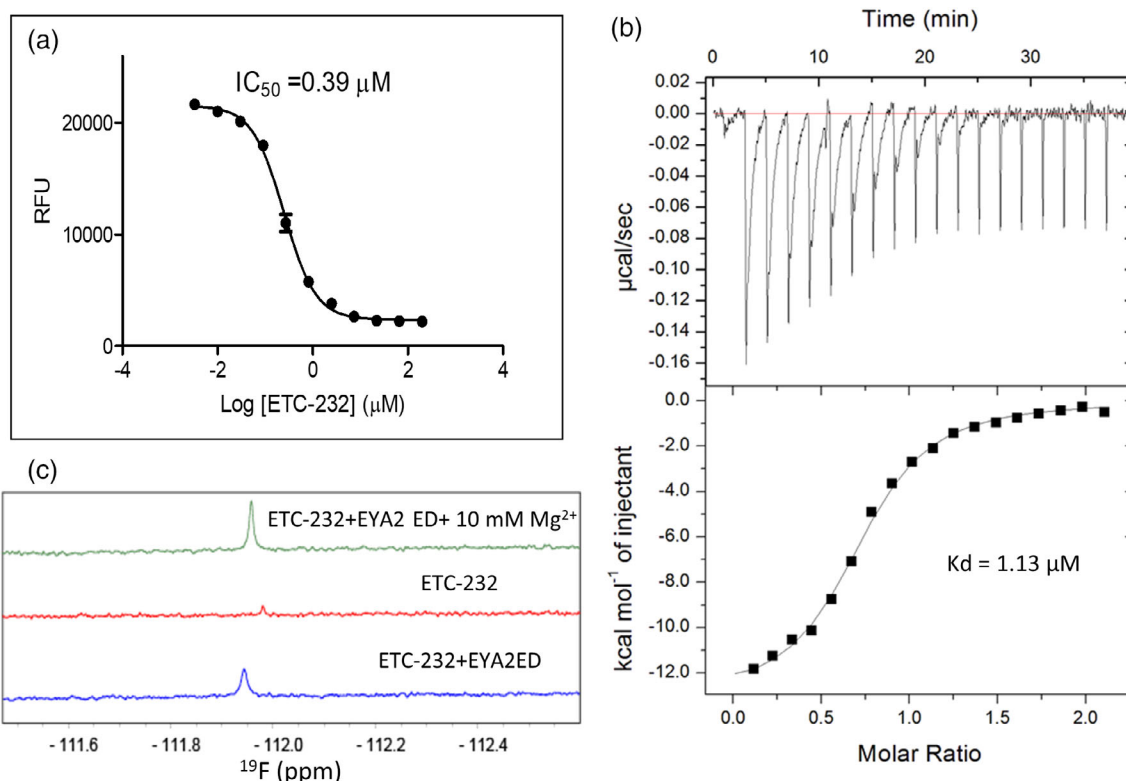


FIGURE 1 The effect of Mg^{2+} on inhibitor binding. (a) The IC_{50} curve of ETC-232. The assay was carried out in the presence of 5 µM Mg^{2+} in the assay buffer. (b) The binding affinity between ETC-232 and EYA2 ED. The protein was prepared in a buffer that contained 20 mM HEPES pH 7.5, 150 mM NaCl, 1 mM DTT, 0.5 mM EDTA. The binding assay was performed at 25°C. (c) Effect of Mg^{2+} on ETC-232 and EYA2 ED interactions. The ¹⁹F-NMR spectra of ETC-232 in the absence (red) and presence of EYA2 ED (blue) and Mg^{2+} (green) are shown. The protein was prepared in a buffer that contained 20 mM HEPES pH 7.5, 150 mM NaCl, 1 mM DTT. The data were collected at 25°C

EYA2 ED, ETC-232 exhibited a peak with a higher intensity (Figure 1c). The shifted resonance was due to its interactions with EYA2 ED, and the increased peak intensity was the result of the increased solubility of ETC-232 in the presence of EYA2 ED. When Mg^{2+} was added into the mixture, ETC-232 exhibited a sharper peak than its bound form, indicating that Mg^{2+} reduced the molecular interactions between ETC-232 and EYA2, releasing ETC-232 into solution.

2.2 | Structure–activity–relationship analysis of the inhibitors

Stemming from ETC-232, we modified three parts of the molecule to improve inhibitor potency: (a) the left-hand side pyrimidine, (b) the hydrazide linker, and (c) the right-hand side fluorobenzene (Figure S1). When pyrimidine was removed, there was a complete loss in activity (ETC-176, IC_{50} >200 µM) against the EYA2 ED Tyr phosphatase activity. Replacing pyrimidine with a phenyl ring (ETC-618, IC_{50} 2.64 µM, Figure 2) resulted in a greater

than fivefold loss in activity. Restoration of the ortho-nitrogen on the phenyl ring, as in analogue ETC-170, resulted in retaining both potency and binding affinity when compared to ETC-232 (ETC-170, IC_{50} 0.55 µM, Figure 2; Figure S2).

To determine whether the binding site would accommodate a ligand with a flexible linker, we reduced the hydrazide linker of ETC-232. This new molecule, named ETC-439, exhibited a >30-fold loss in activity (Figure 2). The same trend was observed with ETC-115, which showed a >300-fold loss in activity when compared to ETC-616 (Figure 2). These results strongly indicate that a rigid bond is essential at the linker region, allowing the ligand to be in an energetically favourable conformation that enables hydrogen bond interactions with Thr278 and Thr421 (Figure S1).

Finally, we attempted to improve potency through modifications on the right-hand side fluorobenzene. The removal of this entire moiety resulted in a complete loss of EYA2 Tyr phosphatase activity (ETC-651, IC_{50} >200 µM, Figure 2). Reinstalling the phenyl ring (ETC-440, IC_{50} 0.87 µM, Figure 2) increased the potency, and

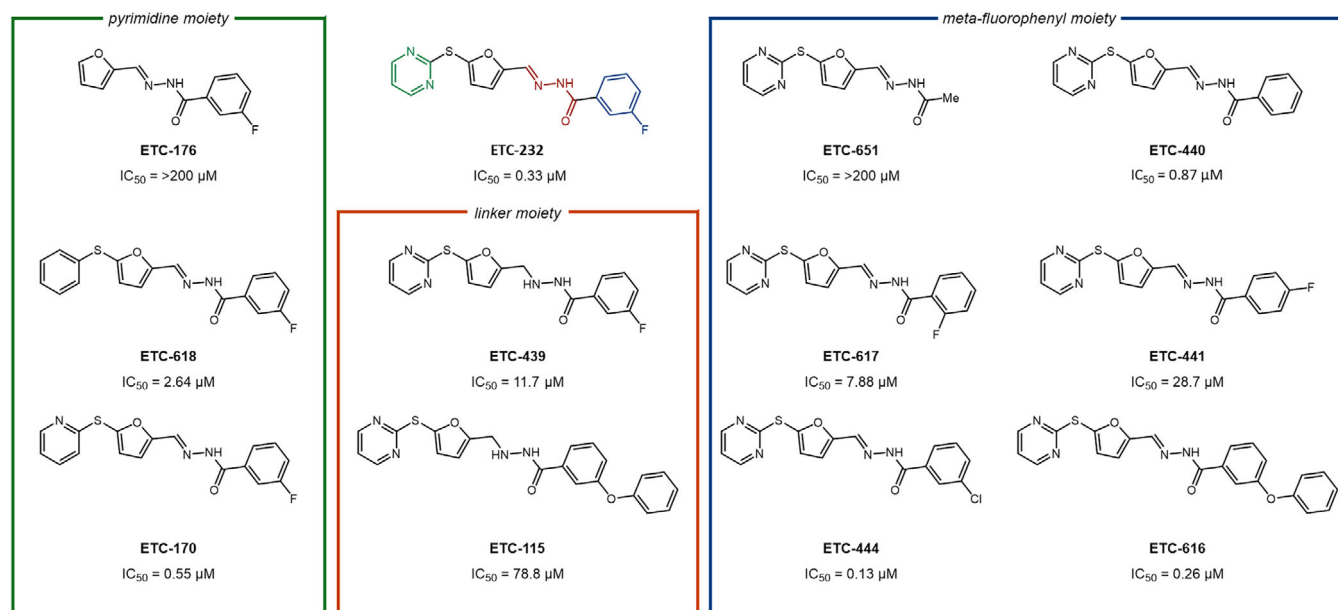


FIGURE 2 Compounds synthesized. Structures and IC₅₀ of the compounds synthesized in this study are shown

fluoro-substitutions around the phenyl ring indicate that the substitution at the meta position is preferred for the activity rather than the ortho and para positions (Figure 2). The analogue ETC-441, containing the fluoro-substitution at the para position, has an IC₅₀ of 28.73 μM in the OMFP assay. The substitution at the para position lowers the IC₅₀ 70×, likely due to a steric clash with Tyr461 (Figure 2). To occupy space available inside the binding pocket (Figure S1), we substituted chlorine for fluorine, which led to a twofold improvement in activity compared to the meta-fluoro substitution (ETC-444, IC₅₀ 0.13 μM, Figure 2). These data indicated that the binding pocket can tolerate a bigger group, and the addition of a phenoxy group (ETC-616, IC₅₀ 0.26 μM, Figure 2) indeed restored the potency. The analogue ETC-616 contains a phenoxy group replacing the fluorine atom of ETC-232. To our surprise, based on the crystal structure of ETC-232 (PDB: 5ZMA),²¹ the limited space interior to the binding tunnel makes it difficult to accommodate the phenoxy extension. A careful examination of the binding site led us to hypothesize that movement of the sidechain from Trp410 would perhaps allow the fit of ETC-616. To further corroborate this hypothesis, we modeled the binding of ETC-616 via molecular docking followed by a 200-ns MD simulation on the docked complex. The MD simulation results show that the phenoxy group from ETC-616 inserts deeply into the binding site to occupy the space created by the movement of W410. π -stacking between Tyr461 and the phenoxy moiety was observed from the MD simulation (Video S1). In conclusion, ETC-444, which has the fluorine to chlorine

substitution, is the most potent EYA2 Tyr inhibitor with an IC₅₀ of 0.13 μM against EYA2 ED activity. In addition, isothermal titration calorimetry (ITC) demonstrated that ETC-444 binds to EYA2 ED with a K_D of 0.52 μM (Figure S3).

2.3 | Co-crystal structures of EYA2 ED with selected inhibitors

According to the published co-crystal structure, ETC-232 binds deeply within the EYA2 ED and affects Mg²⁺ binding.²⁰ The allosteric inhibitor binding pocket was not observed in ligand-free Mg²⁺ bound EYA2 ED.^{5,17} This finding makes structure-based compound optimization challenging, as the pocket might alter its shape to bind to different inhibitors. To further characterize the binding mode for this series of inhibitors, we attempted to determine the crystal structures of EYA2 ED in complex with several of our novel analogues. We managed to solve two co-crystal structures for EYA2 ED in complex with newly designed analogues of ETC-232: ETC-170 and ETC-616 (Figure 3a). The crystal structures of EYA2 ED–ETC-170 and EYA2 ED–ETC-616 complexes were determined at 3.3 Å resolution and 3.5 Å resolution, respectively. Data collection and refinement statistics are shown in Table 1. Overlays of EYA2 ED in complex with ETC-232, ETC-170, and ETC-616 structures show that the binding of ETC-170 and ETC-616 to EYA2 ED does not change the overall structure of EYA2 ED (Figure S4). Similar to ETC-232, ETC-170 and ETC-616 are bound at the interface between the catalytic domain and the helical bundle

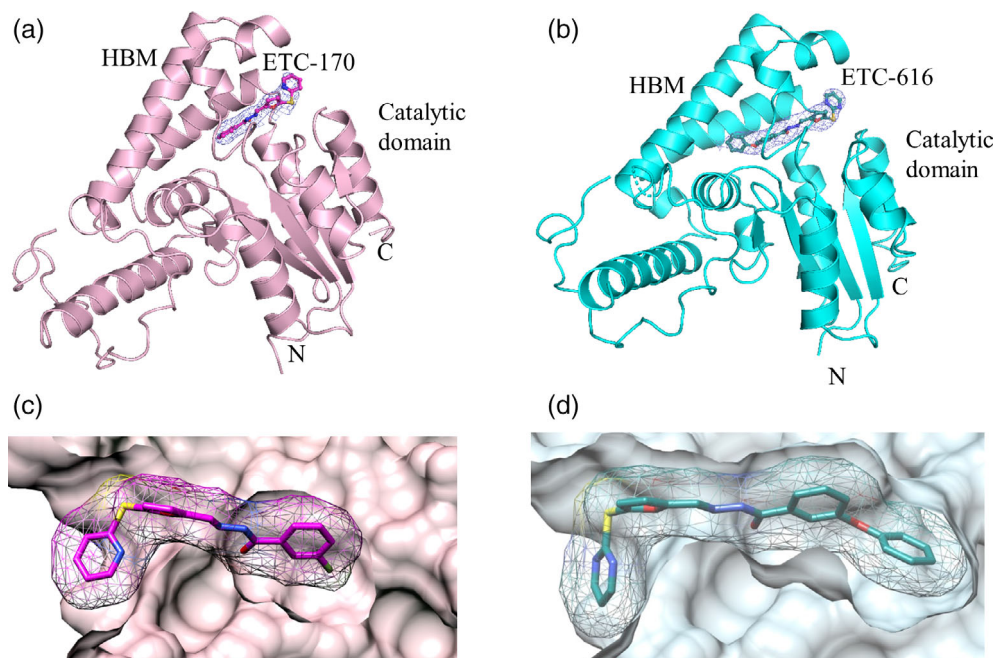


FIGURE 3 Structures of EYA2 ED in complexes with ETC-170 and ETC-616. (a) The overall structures of EYA2 ED–ETC-170 complex (pink). (b) The overall structures of EYA2 ED–ETC-616 complex (cyan). ETC-170 and ETC-616 inhibitors are shown in sticks and the 2Fo–Fc map (contoured at one sigma) for the inhibitors are shown in blue. The induced allosteric binding pocket of EYA2 ED protein upon different ligand binding shown in surface representation and the inhibitors are shown in sticks as in mesh representation ETC-170 (c) and ETC-616 (d)

motif (HBM) by inducing a tunnel-like pocket (Figure 3b). Similar to ETC-232, the binding of ETC-170 and ETC-616 caused significant conformational changes to the catalytically important $\beta 1$ – $\alpha 1$ loop (residues 274–282) containing Motif I (residues 274–278) and the Mg^{2+} coordinating residues (D274, D276, and D502).²³ These conformational changes induced by compound binding are not favourable for Mg^{2+} interaction, thus inhibiting the enzyme. Therefore, the co-crystal structures of ETC-170 and ETC-616 (analogues of ETC-232) to EYA2 ED further confirm the allosteric nature of this class of inhibitors. A more detailed comparison among these analogues is presented below.

2.4 | Structural studies explain SAR of the compounds

The available structures explain the SAR of the compounds and provide insight into further development of this class of inhibitors. First, the left-hand side pyrimidine ring of the inhibitor molecule is partially surrounded by key “gate-keeping” residues and partially solvent exposed. The pyrimidine ring is involved in (a) stacking interactions with Tyr294 and (b) hydrophobic interactions with Phe290 and (c) the hydrogen bond between His523 and nitrogen of pyrimidine ring. Phe290 is the key residue for selectivity of this ligand against EYA2 ED among other EYA isoforms²⁰ (Figure 4a; Figure S5). In ETC-616 and ETC-170 structures, the left side of the ligand retains similar hydrophobic interactions with EYA2 ED. These observations in the

crystal structure along with the SAR demonstrate that pyrimidine is necessary to maintain potency and to act as an “anchor” to position the ligand in the allosteric pocket. Second, in the co-crystal structures, we observed two strong hydrogen bond interactions with the rigid hydrazide linker: one between the carbonyl oxygen of Thr278 and nitrogen of the hydrazide and the other hydrogen bond between the sidechain of Thr421 and carbonyl oxygen of the inhibitor (Figure 4c). The Thr278 of Motif I is located in the catalytically important $\beta 1$ – $\alpha 1$ loop and helps in the positioning of the crucial Asp274 and Asp502 of catalytic triad residues to coordinate a magnesium ion for enzymatic function in the active protein. Upon ligand binding, this class of allosteric inhibitors causes a significant conformational change on the catalytically important $\beta 1$ – $\alpha 1$ loop. This rearrangement positions the carbonyl oxygen of Thr278 to form a hydrogen bond with the hydrazine moiety of these allosteric inhibitors. Across all of the three EYA2 ED-inhibitor (ETC-232, ETC-170, and ETC-616) complex structures, hydrogen bond interactions were observed between carbonyl oxygen of Thr278 and the second nitrogen of the hydrazide linker (Figure 4c). Finally, in the co-crystal structure with ETC-232 and ETC-170, the fluorobenzene on the right-hand side makes π/π interactions with Tyr461 and makes hydrophobic interactions with residues Ile279, Met308, Leu417, and Leu425. When this entire moiety is removed, it results in an inactive compound (ETC-651). This result suggests that the π/π interactions from the phenyl ring with Tyr461 provide binding affinity in the hydrophobic pocket of the EYA2 protein.

TABLE 1 Data collection and refinement statistics

	EYA2 ED-ETC-170 (PDB: 7F8H)	EYA2 ED-ETC-616 (PDB: 7F8G)
Wavelength	0.9998	0.9537
Resolution range	56.0–3.3 (3.418–3.3)	44.96–3.492 (3.617–3.492)
Space group	I 1 2 1	P 31
Number of molecules/ASU	3	2
Unit cell	144.281 50.419 144.281 90 101.846 90	89.919 89.919 96.850 90 90 120
Total reflections	64,318 (11,604)	21,687 (5,221)
Unique reflections	17,269 (3,080)	10,772 (2,611)
Multiplicity ^a	3.7 (3.8)	2.0(2.0)
Completeness (%)	100.0 (100.0)	96.7 (98.0)
Mean I/sigma(I)	6.8 (1.3)	10.7(2.9)
Wilson B-factor	99.06	82.64
R_{merge}^b	0.034 (0.247)	0.091(0.370)
R_{pim}	0.034 (0.247)	0.081(0.333)
CC1/2	0.998 (0.907)	0.991(0.769)
Reflections used in refinement	15,630 (1,511)	10,758 (1,114)
Reflections used for R_{free}	1,565 (151)	1,080 (115)
R_{work}	0.234 (0.319)	0.213 (0.296)
R_{free}^c	0.281 (0.388)	0.267 (0.391)
Number of non-hydrogen atoms	5,980	3,995
Macromolecules; ligands; protein residues	5,908; 72; 778	3,935; 60; 516
RMS(bonds; angles)	0.002; 0.50	0.003; 0.60
Ramachandran favored; allowed; outliers (%)	92.82; 7.18; 0.0	93.28; 6.72; 0.0
Rotamer outliers (%)	0	0.00
Clashscore	6.83	7.80
Average B-factor	101.71	83.35
Macromolecules; ligands	102.00; 77.87	83.62; 65.46

^aStatistics for the highest-resolution shell are shown in parentheses.

^b $R_{\text{merge}} = \sum_h \sum_i |I_{hi} - \langle I_h \rangle| / \sum_h I_{hi}$, where I_{hi} is the i th observation of the reflection h , while $\langle I_h \rangle$ is its mean intensity.

^c R_{free} was calculated with 5% of reflections excluded from the whole refinement procedure.

3 | DISCUSSION

In the current study, we have designed and synthesized novel EYA2 inhibitors based on an available crystal structure of the EYA2 ED in complex with one inhibitor.²⁰ The SAR of these inhibitors has been generated, and our results suggest that the pyrimidine and fluorinated benzene are critical for the activity of the inhibitors (Figure 2). We show that replacing the fluorine atoms with a chloride atom results in a slightly more potent inhibitor (ETC-444) with improved IC_{50} and binding affinity to EYA2 ED (Figure 2). Although we demonstrate that modification on other moieties could generate inhibitors with similar IC_{50} to that of ETC-232, the potency is

not good enough for clinical applications. Our current study implies that challenges remain to optimize this class of inhibitors into drugs. Nonetheless, several compounds with different molecular weights having similar IC_{50} against the EYA2 ED Tyr phosphatase activity were generated in this study. Although these compounds do not disrupt the interaction between SIX1 and EYA2 ED,²⁰ they have the potential to disrupt SIX1/EYA2-mediated transcription, as some SIX1 target genes require the EYA2 Tyr phosphatase.³ Most importantly, these inhibitors can be utilized as chemical probes to evaluate the function of the Tyr phosphatase activity of EYA2 in different cancers. Indeed, in previous work, we used ETC-232 to elucidate the function of the EYA2 Tyr

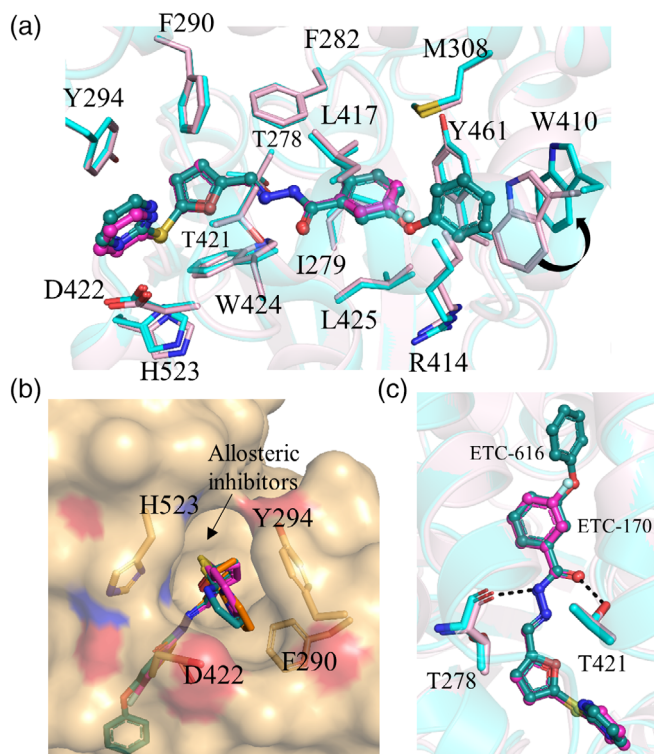


FIGURE 4 Residues critical for inhibitor bindings. (a) Overlay of EYA2 ED in complexes with ETC-170 and ETC-616. Overlay of EYA2 ED–ETC-170 complex (pink) and EYA2 ED–ETC-616 complex (cyan) structures are showing that the positions of the residues ($<4 \text{ \AA}$) that line the binding pocket of inhibitors are similar between these two structures except the residue Trp410. The side chain of Trp410 is pushed farther away to accommodate the phenoxy group of ETC-616 and indicated by an arrow. (b) The allosteric binding pocket of EYA2 ED protein shown in surface representation. The inhibitors and the sidechains of residues that surrounds the pyrimidine ring of the inhibitors are shown in sticks (ETC-232 [wheat], ETC-170 [magenta], and ETC-616 [dark cyan]). (c) The hydrogen bonds between Thr278 and Thr421 of EYA2 ED with hydrazine moiety of inhibitors (ETC-170) and (ETC-616) are shown in dotted lines, and inhibitors are displayed in ball and stick representation

phosphatase activity in human lung cancer and in glioblastoma.^{20,24} Our newly developed compounds might be useful for probing function of EYA2 in different model systems. As several compounds contain a fluorine atom, they could be used to identify more potent inhibitors with novel scaffolds using ^{19}F -NMR spectroscopy.

Our biochemical study showed that a high concentration of Mg^{2+} affects the IC_{50} of ETC-232, suggesting that higher concentrations of Mg^{2+} might be able to prevent the conformational changes in EYA2 ED caused by inhibitor binding. This finding is consistent with our co-crystal structures. As Mg^{2+} is present in living cells, EYA2 ED should be in complex with this metal ion. Therefore, the potency of the compound, in the context of physiologic

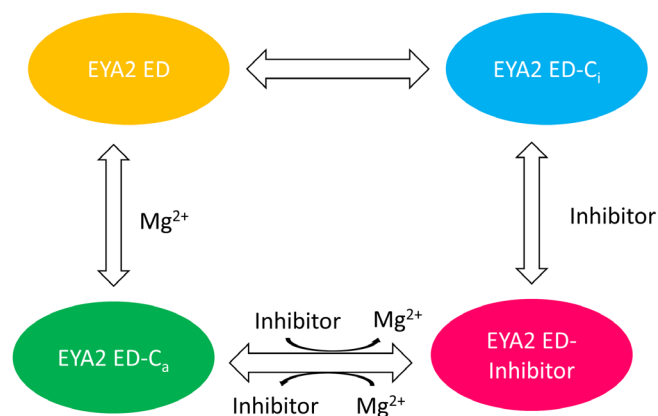


FIGURE 5 Possible conformations of EYA2 ED under physiological conditions. EYA2 ED might contain active (C_a) and inactive conformations (C_i). In the presence of Mg^{2+} , EYA2 ED is in active conformation. The allosteric inhibitor binds to the inactive conformation to form a more stable complex. In addition, an allosteric inhibitor is able to change the confirmation of the active form to release Mg^{2+}

levels of Mg^{2+} , needs to be further improved as the concentration of Mg^{2+} in the cytosol can be in the mM (0.1–1 mM) range.²⁵ Nonetheless, the on-target effect of this type of inhibitor observed in different cells proves that these allosteric inhibitors are able to suppress the enzymatic activity of EYA2 ED under physiological conditions.^{20,24} In addition, our results suggest that the EYA2 ED might exist in active and inactive conformations depending on the presence or absence of Mg^{2+} , while inhibitor binding stabilizes the inactive conformation (Figure 5). It would be useful to explore the conformational exchanges of EYA2 ED using other methods.

Active sites of phosphatases are highly undruggable due to the positively charged residues binding to the phosphorylated substrate.²⁶ The charges of residues in the active site make it challenging to develop potent small molecules, which are usually hydrophobic to have suitable selectivity and cell permeability. It has been proposed that fragment-based approaches can be utilized to develop bivalent ligands that can overcome the challenges.²⁶ Our current study provides another strategy to develop phosphatase inhibitors. Based on our structural studies, a new druggable pocket was identified. This pocket serves as a new target for developing inhibitors using structure-based drug design. Inhibitors binding to this pocket can also be identified using the compounds presented in current study as a reference molecule.^{27,28} Our structural study shows that the allosteric pocket on EYA2 is suitable for developing small-molecule inhibitors, which may be applicable to other EYA proteins.

In our previous study, we elucidated the structure of the EYA2 ED–ETC-232 complex while in the presence of

EDTA. We hypothesized from this work that the affinity of EYA2 ED to our allosteric ligand was low when compared to the affinity of EYA2 to Mg^{2+} under physiological concentrations. Surprisingly, the co-crystal structure of the EYA2 ED–ETC-170 complex was obtained from a protein sample in the presence of 5 mM $MgCl_2$, without the addition of EDTA. Despite the presence of $MgCl_2$ in the protein sample buffer, electron density for Mg^{2+} was not observed in the EYA2 ED–ETC-170 complex. These data demonstrate that our allosteric inhibitors can bind to the EYA2 ED even in the absence of EDTA and presence of $MgCl_2$, which is consistent with our functional data that show that the Tyr phosphatase activity can be inhibited by our compounds in cells. As the structure and catalysis mechanism of EYA2 are very similar to other phosphatases, multiple conformations might exist in other types of phosphatases. Developing allosteric inhibitors is, thus, a feasible strategy for these undruggable targets. To identify an allosteric inhibitor of a particular phosphatase, high-throughput screening is the preferred method, and conditions, such as concentration of Mg^{2+} , for Mg^{2+} -dependent phosphatases, need to be carefully considered.

In summary, we have studied the SAR of a novel class of EYA2 Tyr phosphatase inhibitors. A number of compounds derived from ETC-232 were evaluated, and ETC-444 exhibited improved IC_{50} against the EYA2 ED Tyr phosphatase activity. Our co-crystal structures reveal the binding modes of the newly developed inhibitors and provide important information for further optimization of this type of inhibitors. We show that EYA2 ED exists in multiple conformations and further demonstrate the roles of Mg^{2+} and the inhibitors in driving EYA2 ED to different conformations. Our study will be helpful for developing EYA2 Tyr phosphatase inhibitors and provide several compounds that can be used as chemical probes.

4 | MATERIALS AND METHODS

4.1 | Protein expression and purification for crystallization

EYA2 ED composing residues 253–538 of human EYA2 was cloned into pGEX6P-1 and purified as described previously.²² In brief, recombinant protein was induced in *Escherichia coli* and purified on a gravity column fill in with glutathione resin. Purified protein was mixed with PreScission protease. The fusion GST tag was removed by gel filtration chromatography. Protein was in a buffer containing 20 mM HEPES 7.5, 150 mM NaCl, and 1 mM DTT. Protein was concentrated and kept at $-80^{\circ}C$ after frozen in liquid nitrogen for long-term storage.

4.2 | Phosphatase assay

The IC_{50} for EYA2 inhibitors was performed in 30 μ l volume in 384-well plates (Greiner) with the following buffer conditions: 50 mM MES, pH 6.5, 50 mM NaCl, 5 μ M $MgCl_2$, and 1 mM DTT. The test compounds were serially diluted threefold from 6 mM to 0.1 μ M in 100% DMSO and subsequently further diluted at a 1:1 ratio in assay buffer; 2.0 μ l of this intermediate compound stock was added to 26 μ l of EYA2 ED enzyme, and the plate was centrifuged at 1500 rpm for 1 min and incubated at RT for 30 min in a shaker (Orbit 300 Multi Purpose Vortexer from Labnet) at 20 rpm; 2 μ l of substrate (OMFP, Sigma-Aldrich, Cat No. M2629-1G) at 1.5 mM concentration prepared in 25% DMSO was added to all the wells and further incubated at RT for 1 hr with shaking. The final concentration of enzyme and substrate was 800 nM and 100 μ M, respectively. Fluorescence intensity was measured (λ_{ex} 485 nm and λ_{em} 515 nm) on a Tecan Infinite M200 pro plate reader. IC_{50} values were determined by fitting the data to the four-parameter dose-response equation using Prism software (GraphPad).

4.3 | Crystallization and structure determination

To study the effect of Mg^{2+} in protein-inhibitors complex formation, the purified EYA2 ED protein sample in gel filtration buffer that contained 20 mM HEPES 7.5, 150 mM NaCl, and 1 mM DTT was exchanged with two different buffer conditions before co-crystallization experiments. One buffer containing Mg^{2+} (HEPES pH 7.5, 200 mM NaCl, 5 mM TCEP, 5 mM $MgCl_2$, and 5% glycerol) and in the other buffer contain the presence of EDTA (HEPES pH 7.5, 200 mM NaCl, 5 mM TCEP, 0.5 mM EDTA, and 5% glycerol). The protein-inhibitor complex solution was prepared by mixing the protein EYA2 ED with inhibitors in 1:2 molar ratio. The crystals of protein-inhibitor complexes were grown in a sitting drop containing 1 μ l of protein and 1 μ l of reservoir solution at $20^{\circ}C$. The EYA2 ED–ETC-170 was crystallized in buffer containing 0.2 M sodium citrate tribasic dihydrate, 20% PEG 3350. The crystals of EYA2 ED–ETC-616 complex were obtained from crystallization buffer 0.02 M $MgCl_2$, 0.1 M HEPES 7.5, and 22% poly acrylic acid sodium salt 5100. For cryoprotection, the crystals were shortly soaked in well solution supplemented with 25% glycerol and flash frozen in liquid nitrogen.

The X-ray diffraction datasets for EYA2 ED–ETC-170 and EYA2 ED–ETC-616 were collected at NSRRC TPS 05A at Taiwan and MX2 beamline at the Australian Synchrotron, respectively. The collected datasets for EYA2

ED-ETC-170 and EYA2 ED-ETC-616 complexes were processed and scaled using HKL2000 and XDS, respectively.^{21,25} The co-crystal structures were determined using EYA2 ED-ETC-232 structure (PDB: 5ZMA) as initial model by the molecular replacement method in PHENIX.²⁴ Further model building and iterative refinement were performed using COOT and PHENIX, respectively.^{22,24} The refinement and structure validation statistics are shown in Table 1.

4.4 | ¹⁹F-NMR spectroscopy

¹⁹F-NMR spectroscopy was obtained on a Bruker 400 MHz equipped with a BBO probe at 25°C. Standard 1D ¹⁹F-NMR was acquired and processed using Topspin (4.0).²⁹ ETC-232 was prepared to a final concentration of 100 μM in assay buffer that contained 20 mM HEPES pH 7.5, 150 mM NaCl, 1 mM DTT. The NMR spectra of ETC-232 in the absence and presence of 50 μM EYA2 ED were collected. To detect effect of Mg²⁺ on the ligand binding, 10 mM Mg²⁺ was added into EYA2, followed by the data collection. To remove the metal ions possibly binding to EYA2 ED, the purified protein was treated with EDTA followed by purification with of the assay buffer.

4.5 | Isothermal titration calorimetry studies

ITC experiment was performed on an Auto-iTC200 instrument (Microcal Inc.) at 25°C. Protein was prepared in 20 mM HEPES pH 7.5, 150 mM NaCl, 1 mM DTT, 0.5 mM EDTA to a final concentration of 20 μM (400 μl, cell) and compounds were dissolved in the same buffer to a final concentration of 150–300 μM (200 μl, titrant). The titration experiments were carried out with 18 injections over a period of 40 min with stirring at 1000 rpm. The binding was analysed using single site-binding mode. The dissociation constant (Kd) and other parameters were determined using Origin provided with the instrument.

4.6 | Molecular docking

The W410A mutated EYA2 (PDB: 5ZMA) was submitted to the Protein Preparation Wizard where atom and bond types were corrected, and protonation states of ionizable species adjusted to pH 7.4 by Epik. The ligand ETC-616 was constructed based on the coordinates of ETC-232 from its co-crystal structure with EYA2. The Glide docking program from Schrödinger suite was used for setting up grid file for docking. During receptor grid generation,

the ligand to be docked was confined to an enclosing box centred on the ETC-232 from the co-crystal structure with an inner box size of 10 Å × 10 Å × 10 Å and an outer box size of 26.85 Å × 26.85 Å × 26.85 Å. The “Refine only” mode was applied with Standard Precision mode during the docking stage.

4.7 | Molecular dynamic stimulations

Molecular dynamic simulations were performed with Desmond Molecular Dynamics System (D.E. Shaw Research). The docked complex of ETC-616 and EYA2 (PDB: 5ZMA) was solvated in an orthorhombic box with solvent buffers of 10 Å along each dimension. The TIP3P solvent model was used to describe water molecules. Overall neutralization of the system was achieved by adding sodium and chloride ions at a physiological concentration of 0.15 M. The prepared model systems were then relaxed with a multistep default protocol in Desmond. After relaxation, the whole system was subjected to a 200-ns simulation production. The OPLS-AA/2005 force-field parameters were implemented during simulations. The SHAKE algorithm was used to constrain the bond length of hydrogen atoms. Long-range electrostatic forces were calculated with the particle-mesh Ewald method. The cutoff distance for computing short-range electrostatics and Lennard-Jones interaction was set to 9.0 Å.

ACKNOWLEDGMENTS

The authors appreciate the valuable suggestion from our colleagues at EDDC.

CONFLICT OF INTEREST

The authors declare no competing interests.

AUTHOR CONTRIBUTIONS

Jothi Anantharajan: Data curation (lead); writing – review and editing (equal). **Nithya Baburajendran:** Data curation (supporting); supervision (supporting). **Grace Lin:** Data curation (lead). **Yong Yao Loh:** Data curation (supporting); writing – review and editing (supporting). **Weijun Xu:** Data curation (supporting); writing – review and editing (supporting). **Nur Huda Binte Ahmad:** Data curation (supporting). **Shuang Liu:** Data curation (supporting); writing – original draft (supporting). **Anna Jansson:** Data curation (supporting); supervision (supporting). **John Kuan:** Data curation (lead). **Elizabeth Ng:** Data curation (supporting). **Yee Khoon Yeo:** Data curation (supporting). **Alvin Huang:** Data curation (supporting); supervision (supporting). **Jeffery Hill:** Supervision (supporting). **Heide Ford:**

Supervision (supporting); writing – review and editing (supporting). **Rui Zhao**: Supervision (supporting); writing – review and editing (supporting). **Congbao Kang**: Project administration (lead); resources (supporting); writing – original draft (lead).

ORCID

CongBao Kang  <https://orcid.org/0000-0002-9886-9374>

REFERENCES

- Kumar JP. The sine oculis homeobox (SIX) family of transcription factors as regulators of development and disease. *Cell Mol Life Sci.* 2009;66:565–583.
- Christensen KL, Patrick AN, McCoy EL, Ford HL. The six family of homeobox genes in development and cancer. *Adv Cancer Res.* 2008;101:93–126.
- Blevins MA, Towers CG, Patrick AN, Zhao R, Ford HL. The SIX1-EYA transcriptional complex as a therapeutic target in cancer. *Expert Opin Therapeut Targets.* 2015;19:213–225.
- Vartuli RL, Zhou H, Zhang L, et al. Eya3 promotes breast tumor-associated immune suppression via threonine phosphatase-mediated PD-L1 upregulation. *J Clin Invest.* 2018;128:2535–2550.
- Zhang L, Zhou H, Li X, et al. Eya3 partners with PP2A to induce c-Myc stabilization and tumor progression. *Nat Commun.* 2018;9:1047.
- Zhou H, Zhang L, Vartuli RL, Ford HL, Zhao R. The Eya phosphatase: Its unique role in cancer. *Int J Biochem Cell Biol.* 2018;96:165–170.
- Farabaugh SM, Micalizzi DS, Jedlicka P, Zhao R, Ford HL. Eya2 is required to mediate the pro-metastatic functions of Six1 via the induction of TGF- β signaling, epithelial-mesenchymal transition, and cancer stem cell properties. *Oncogene.* 2012;31:552–562.
- Patrick AN, Cabrera JH, Smith AL, Chen XS, Ford HL, Zhao R. Structure-function analyses of the human SIX1-EYA2 complex reveal insights into metastasis and BOR syndrome. *Nat Struct Mol Biol.* 2013;20:447–453.
- Huang YT, Heist RS, Chirieac LR, et al. Genome-wide analysis of survival in early-stage non-small-cell lung cancer. *J Clin Oncol.* 2009;27:2660–2667.
- Yuan Y, Zheng S, Li Q, et al. Overexpression of miR-30a in lung adenocarcinoma A549 cell line inhibits migration and invasion via targeting EYA2. *Acta Biochim Biophys Sin (Shanghai).* 2016;48:220–228.
- Li Z, Qiu R, Qiu X, Tian T. EYA2 promotes lung cancer cell proliferation by downregulating the expression of PTEN. *Oncotarget.* 2017;8:110837–110848.
- Liang Y, Xu X, Wang T, et al. The EGFR/miR-338-3p/EYA2 axis controls breast tumor growth and lung metastasis. *Cell Death Dis.* 2017;8:e2928.
- Mimae T, Okada M, Hagiya M, et al. Upregulation of notch2 and six1 is associated with progression of early-stage lung adenocarcinoma and a more aggressive phenotype at advanced stages. *Clin Cancer Res.* 2012;18:945–955.
- Xia Y, Zhu Y, Ma T, et al. miR-204 functions as a tumor suppressor by regulating SIX1 in NSCLC. *FEBS Lett.* 2014;588:3703–3712.
- Zhou H, Blevins MA, Hsu JY, et al. Identification of a small-molecule inhibitor that disrupts the SIX1/EYA2 complex, EMT, and metastasis. *Cancer Res.* 2020;80:2689–2702.
- Li X, Ohgi KA, Zhang J, et al. Eya protein phosphatase activity regulates Six1-Dach-Eya transcriptional effects in mammalian organogenesis. *Nature.* 2003;426:247–254.
- Rayapureddi JP, Kattamuri C, Steinmetz BD, et al. Eyes absent represents a class of protein tyrosine phosphatases. *Nature.* 2003;426:295–298.
- Tootle TL, Silver SJ, Davies EL, et al. The transcription factor eyes absent is a protein tyrosine phosphatase. *Nature.* 2003;426:299–302.
- Jung SK, Jeong DG, Chung SJ, et al. Crystal structure of ED-Eya2: Insight into dual roles as a protein tyrosine phosphatase and a transcription factor. *FASEB J.* 2010;24:560–569.
- Anantharajan J, Zhou H, Zhang L, et al. Structural and functional analyses of an allosteric EYA2 phosphatase inhibitor that has on-target effects in human lung cancer cells. *Mol Cancer Ther.* 2019;18:1484–1496.
- Pandey RN, Rani R, Yeo EJ, et al. The eyes absent phosphatase-transactivator proteins promote proliferation, transformation, migration, and invasion of tumor cells. *Oncogene.* 2010;29:3715–3722.
- Krueger AB, Drasin DJ, Lea WA, et al. Allosteric inhibitors of the Eya2 phosphatase are selective and inhibit Eya2-mediated cell migration. *J Biol Chem.* 2014;289:16349–16361.
- Tonks NK. Protein tyrosine phosphatases: From genes, to function, to disease. *Nat Rev Mol Cell Biol.* 2006;7:833–846.
- Zhang G, Dong Z, Gimple RC, et al. Targeting EYA2 tyrosine phosphatase activity in glioblastoma stem cells induces mitotic catastrophe. *J Exp Med.* 2021;218:e20202669.
- Murphy E. Mysteries of magnesium homeostasis. *Circ Res.* 2000;86:245–248.
- Zhang Z-Y. Drugging the undruggable: Therapeutic potential of targeting protein tyrosine phosphatases. *Acc Chem Res.* 2017;50:122–129.
- de Castro GV, Ciulli A. Spy vs. spy: Selecting the best reporter for 19F NMR competition experiments. *Chem Commun.* 2019;55:1482–1485.
- Kang CB. 19F-NMR in target-based drug discovery. *Curr Med Chem.* 2019;26:4964–4983.
- Li Y, Wong YL, Ng FM, et al. Characterization of the interaction between Escherichia coli topoisomerase IV E subunit and an ATP competitive inhibitor. *Biochem Biophys Res Commun.* 2015;467:961–966.

SUPPORTING INFORMATION

Additional supporting information may be found in the online version of the article at the publisher's website.

How to cite this article: Anantharajan J, Baburajendran N, Lin G, Loh YY, Xu W, Ahmad NHB, et al. Structure–activity relationship studies of allosteric inhibitors of EYA2 tyrosine phosphatase. *Protein Science.* 2022;31:422–31. <https://doi.org/10.1002/pro.4234>